Wind Tunnel Testing of Passive High-Lift Systems

Mihai Victor PRICOP*[,1], Corneliu STOICA[1], Catalin NAE[1], Florin MUNTEANU[2], Jean-Pierre ROSENBLUM[3], Andreea BOBONEA[1], Ionut BRINZA[1]

*Corresponding author
*[,1]INCAS – National Institute for Aerospace Research "Elie Carafoli"
B-dul Iuliu Maniu 220, Bucharest 061126, Romania
vpricop@incas.ro
[2] Aerospace Consulting
B-dul Iuliu Maniu 220, Bucharest 061126, Romania
[3] Dassault Aviation, Direction Generale Technique
78 Quai Marcel Dassault, 92552 Saint-Cloud Cedex 300, France

DOI: 10.13111/2066-8201.2012.4.1.8

Abstract: *This paper presents experimental results obtained with passive high lift systems using a combination of smart flap kinematics and vortex generators. A mid-scale 2.5D wind tunnel model based on DLR-F15 is tested in INCAS Subsonic Wind Tunnel, swept at 30 deg, incorporating the slat, 54 flap/VG/chord extension configurations and test matrix, developed by Dassault-Aviation. INCAS designed, manufactured and instrumented components to be added to the existing INCAS-F15 2D wind tunnel model. The test campaign was completed and results are presented.*

Key Words: *high lift system, wind tunnel, vortex generator, smart kinematics flap*

1. INTRODUCTION

Nomenclature

CL_i – lift coefficient; i=max indicates maximum value;

Cd – drag coefficient;

α_i – incidence angle; index meaning: b=balance, w=streamwise reference system incidence, 0=offset incidence;

β_b – yaw angle;

MVG_i – mechanical vortex generator, as in Fig. 2;

ME – chord max extension, as in Fig. 2.

The purpose of this work is to evaluate in the wind tunnel the major features of smart kinematics flap technology for a DLR-F15 2.5D model at Reynolds 2 Million.

The experimental program was designed accordingly, where key elements considered were as follows:

- 2.5D flow type;
- Chord length of about 0.7m, span 2.07m, sweep angle 30deg, aspect ratio 2.89;
- Global loads are measured using a 6 - component external balance;
- Local pressure distribution is measured using a scanning system in 2 sections for the main element and one section for flap and slat;
- Flow separation is to be evaluated using tufts, oil visualization techniques and from pressure distributions;
- The wind tunnel campaign was considered for Reynolds 2 million.

Various flap/gap, chord extension and vortex generators combinations are assessed.

2. TEST PROGRAM DEFINITION

Take Off, Landing and intermediate configurations were prepared/measured. Two chord extensions, called max extension 75% and 100% are combined with various Vortex Generators, see Fig. 2, called MVG1/3 for flap (7% from and normal to the leading edge) and MVG2/4 for main element of the wing (15 deg with respect to the flow), as indicated in [9]. Tabbed flap, double slotted flap are included in tests, also combined with Max. extension 75%.

No.	Setting	configuration	flap setting or flap1/flap2 or flap/tab	flap gap	flap overlap	Vortex generators	AOA°	Speed (m/s)	tufts	balance measurement	pressure measurements
1	1	Reference	20°	5,9 mm	27 mm	no	[-5, 25]	40	yes	yes	yes
2	2	Reference	40°	10 mm	3,3 mm	no	[-5, 25]	40	yes	yes	yes
3	3	Reference	40°	7,5 mm	11 mm	no	[-5, 25]	40	yes	yes	yes
4	4	Reference	40°	11,8 mm	"-2,3 mm"	no	[-5, 25]	40	yes	yes	yes
5	5	Reference	40°	7,5 mm	3,3 mm	no	[-5, 25]	40	yes	yes	yes
6	6	Reference	40°	13,5 mm	3,3 mm	no	[-5, 25]	40	yes	yes	yes
7	7	Reference	48°	15,9 mm	3,3 mm	no	[-5, 25]	40	yes	yes	yes
8	3	Reference	40°	7,5 mm	11 mm	MVG1	[-5, 25]	40	yes	yes	yes
9	4	Reference	40°	11,8 mm	"-2,3 mm"	MVG1	[-5, 25]	40	yes	yes	yes
10	3	Reference	40°	7,5 mm	11 mm	MVG1 & MVG2	[-5, 25]	40	yes	yes	yes
11	4	Reference	40°	11,8 mm	"-2,3 mm"	MVG1 & MVG2	[-5, 25]	40	yes	yes	yes
12	3	Reference	40°	7,5 mm	11 mm	MVG1 & MVG4	[-5, 25]	40	yes	yes	yes
13	4	Reference	40°	11,8 mm	"-2,3 mm"	MVG1 & MVG4	[-5, 25]	40	yes	yes	yes
13X	4	Reference	40°	11,8 mm	"-2,3 mm"	MVG4	[-5, 25]	40	yes	yes	yes
14	3	Reference	40°	7,5 mm	11 mm	MVG3	[-5, 25]	40	yes	yes	yes
15	4	Reference	40°	11,8 mm	"-2,3 mm"	MVG3	[-5, 25]	40	yes	yes	yes
16	8	Max extension 75%	20°	10 mm	3,3 mm	no	[-5, 25]	40	yes	yes	yes
17	9	Max extension 75%	30°	10 mm	3,3 mm	no	[-5, 25]	40	yes	yes	yes
18	10	Max extension 75%	40°	10 mm	3,3 mm	no	[-5, 25]	40	yes	yes	yes
19	11	Max extension 75%	48°	10 mm	3,3 mm	no	[-5, 25]	40	yes	yes	yes
20	12	Max extension 100%	20°	10 mm	3,3 mm	no	[-5, 25]	40	yes	yes	yes
21	13	Max extension 100%	25°	10 mm	3,3 mm	no	[-5, 25]	40	yes	yes	yes
22	14	Max extension 100%	30°	10 mm	3,3 mm	no	[-5, 25]	40	yes	yes	yes
23	15	Max extension 100%	35°	10 mm	3,3 mm	no	[-5, 25]	40	yes	yes	yes
24	16	Max extension 100%	40°	10 mm	3,3 mm	no	[-5, 25]	40	yes	yes	yes
25	17	Max extension 100%	48°	10 mm	3,3 mm	no	[-5, 25]	40	yes	yes	yes
26	16	Max extension 100%	40°	10 mm	3,3 mm	MVG1	[-5, 25]	40	yes	yes	yes
27	16	Max extension 100%	40°	10 mm	3,3 mm	MVG1 & MVG4	[-5, 25]	40	yes	yes	yes
28	16	Max extension 100%	40°	10 mm	3,3 mm	MVG4	[-5, 25]	40	yes	yes	yes
29	16	Max extension 100%	40°	10 mm	3,3 mm	MVG3	[-5, 25]	40	yes	yes	yes
30	17	Max extension 100%	48°	10 mm	3,3 mm	MVG3	[-5, 25]	40	yes	yes	yes
31	18	Max extension 75% + double slotted flap	30°/50°	10 mm	3,3 mm	no	[-5, 25]	40	yes	yes	yes
32	19	Max extension 75% + double slotted flap	30°/60°	10 mm	3,3 mm	no	[-5, 25]	40	yes	yes	yes
33	20	Reference+flap with tab	20°/10°	5,9 mm	27 mm	no	[-5, 25]	40	yes	yes	yes
34	21	Reference+flap with tab	20°/20°	5,9 mm	27 mm	no	[-5, 25]	40	yes	yes	yes
35	22	Reference+flap with tab	40°/10°	10 mm	3,3 mm	no	[-5, 25]	40	yes	yes	yes
36	23	Reference+flap with tab	40°/20°	10 mm	3,3 mm	no	[-5, 25]	40	yes	yes	yes
37	24	Reference+flap with tab	40°/30°	10 mm	3,3 mm	no	[-5, 25]	40	yes	yes	yes
38	25	Reference+flap with tab	40°/40°	10 mm	3,3 mm	no	[-5, 25]	40	yes	yes	yes
39	23	Reference+flap with tab	40°/20°	10 mm	3,3 mm	MVG1	[-5, 25]	40	yes	yes	yes
40	24	Reference+flap with tab	40°/30°	10 mm	3,3 mm	MVG1	[-5, 25]	40	yes	yes	yes
41	26	Reference + double slotted used as tab	40°/20°	10 mm	3,3 mm	no	[-5, 25]	40	yes	yes	yes
42	27	Reference + double slotted used as tab	40°/30°	10 mm	3,3 mm	no	[-5, 25]	40	yes	yes	yes
43	17	Max extension 100%	48°	10 mm	3,3 mm	MVG1	[-5, 25]	40	yes	yes	yes
44	17	Max extension 100%	48°	10 mm	3,3 mm	MVG1 & MVG4	[-5, 25]	40	yes	yes	yes
45	17	Max extension 100%	48°	10 mm	3,3 mm	MVG4	[-5, 25]	40	yes	yes	yes
46	28	Max. ext. 100% + flap/tab	40°/10°	10 mm	3,3 mm		[-5, 25]	40		yes	yes
47	29	Max. ext. 100% + flap/tab	40°/20°	10 mm	3,3 mm		[-5, 25]	40		yes	yes
48	28	Max. ext. 100% + flap/tab	40°/10°	10 mm	3,3 mm	MVG1	[-5, 25]	40		yes	yes
49	29	Max. ext. 100% + flap/tab	40°/20°	10 mm	3,3 mm	MVG1	[-5, 25]	40		yes	yes
50	30	Max. ext. 75% + flap/tab	40°/10°	10 mm	3,3 mm		[-5, 25]	40		yes	yes
51	31	Max. ext. 75% + flap/tab	40°/20°	10 mm	3,3 mm		[-5, 25]	40		yes	yes
52	30	Max. ext. 75% + flap/tab	40°/10°	10 mm	3,3 mm	MVG1	[-5, 25]	40		yes	yes
53	31	Max. ext. 75% + flap/tab	40°/20°	10 mm	3,3 mm	MVG1	[-5, 25]	40		yes	yes

Fig. 1 The final Test matrix

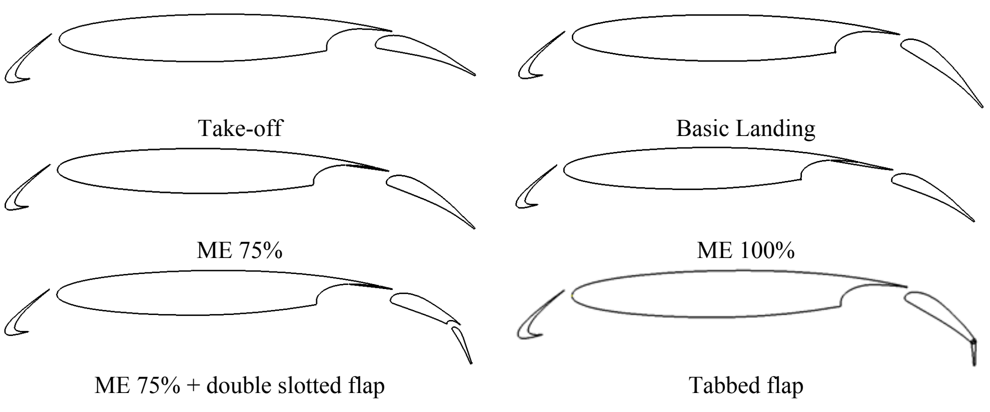

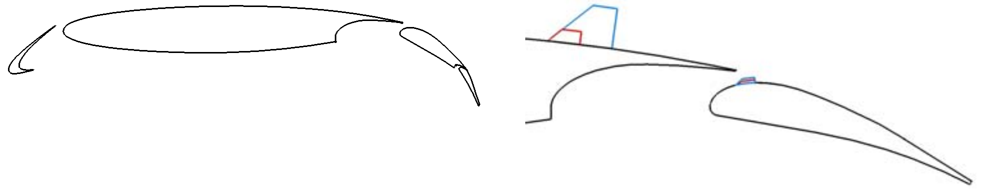

Double slotted used as tab VG – passive vortex generator

Fig. 2 Configuration families; variation is by flap setting and VG configurations

3. WIND TUNNEL, MODEL, INSTRUMENTATION AND TOOLS DESCRIPTION

The INCAS Subsonic Wind Tunnel is an atmospheric, return type, closed-throat, subsonic wind tunnel with a test section of 2.0m high, 2.5m wide and 6m long. Maximum velocity in the test section is more than 110 m/s in low blockage conditions. The test section has an octogonal cross section. The fan is located at the end of the first diffuser, just ahead of the first corner, as in Fig. 3.

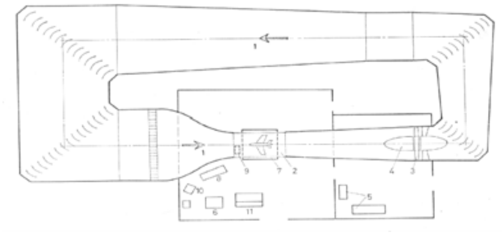

Fig. 3 INCAS Subsonic Wind Tunnel – Aerodynamic circuit

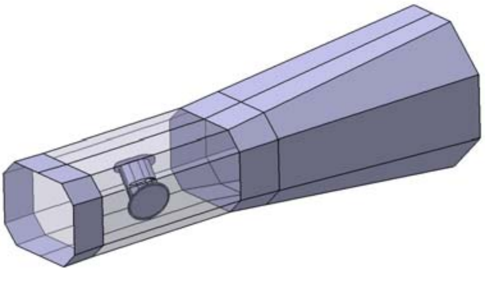

Fig. 4 Model in the test section

The test section has a large amount of plexiglass-paned optical access for virtually all flow visualization techniques and positions. The test section has been designed for complex capability of measuring wall pressure signatures. An under floor six-component, pyramidal external balance T.E.M. is available for use. It can quickly position the models in both pitch and yaw axis over a large motion range. 192 pressure channels of 1, 2.5, 5 or 10 psid data are available.

Model design and manufacturing

The main element of the wing, lower covers, slat, single slotted flap, double slotted and tabbed flaps are machined in 7075 alloy.

The triangular span extensions of the main element have an inner Aluminum structure, enclosed by machined plastic covers.

Chord extensions are composite – carbon/epoxy. Simple wood endplates were designed in an iterative process, to be able to explore a significant range of incidence, in order to capture the stall.

Model Instrumentation

The INCAS F15 wing and flap were instrumented for pressure coefficient measurements by means of 4 x 48 port model D scanivalves installed inside the wing model as in figure below (main wing) and 4x16 DSA digital scanning systems for the wake rake.

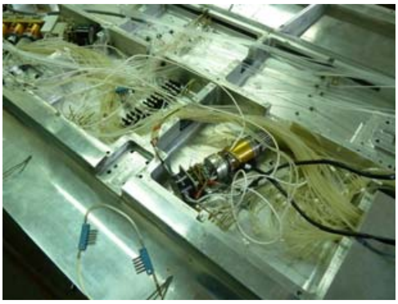

Fig. 5 The mechanical scanivalves installed in the wing model

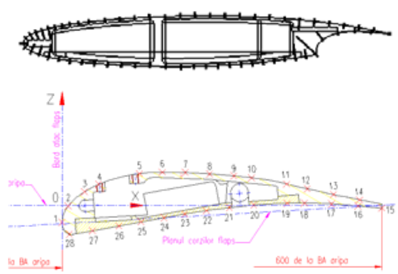

Fig. 6 Position of pressure orifices on wing and flap models (61-68 main element, 28 flap-31, 11 slat)

A total of 59 pressure taps (1 mm diameter, 34 orifices on the upper surface and 25 on the lower surface) were prepared on the wing model in 2 rows – central, streamlined and secondary, 30 deg deflected. The main advantage of the old mechanical scanivalves is the possibility to change the transducer. This way, a range of transducers can be installed, from 1 to 10 PSI or more, depending on the pressure range in the test. Modern pressure scanning arrays have smart functions regarding digitization, calibration, time efficiency, but there is no possibility to change the transducer elements to higher value, being dedicated instruments to a given range. In high-lift applications, a value of -25 for Cp is sometimes achievable for the leading edge area, requesting a proper distribution of transducers versus pressure range.

Data post-processing

Three types of results are available: balance forces and moments, airfoil and wake rake pressure distributions. Each of data has its own corresponding routines. Labview is used to acquire all these data-sets. A typical test means measurement of all in an AoA sweep for a given set of angles. Specific text files are provided, named by the reading (scanning) number: forces and moments - xxxxfm.lvm, airfoil pressures - xxxx.lvm, airfoil Labview time averaged airfoil pressures xxxx_cpmed.lvm and wake rake pressures xxxx_dsa.txt. A FORTRAN code has been written, to coherently process all the dataset. Forces and moments are derived in wind axis reference system. A rotation is applied, since for this campaign, the balance has a 30deg deflection in the horizontal plane, as in [6]. Stream-wise fixing angle of the wing was found to be as in (1).

$$\alpha_w = \arctan\left(\tan(\alpha_b - \alpha_0)\cos(\beta_b)\right) \tag{1}$$

Classical solid wall corrections [1], [2], [3] are applied, using the existing methodology/routines available. Standard blockage corrections of force/moment coefficients, dynamic pressure, Mach, Reynolds, are applied: wake and separation effects are included. Lift, incidence and pitching moment are corrected.

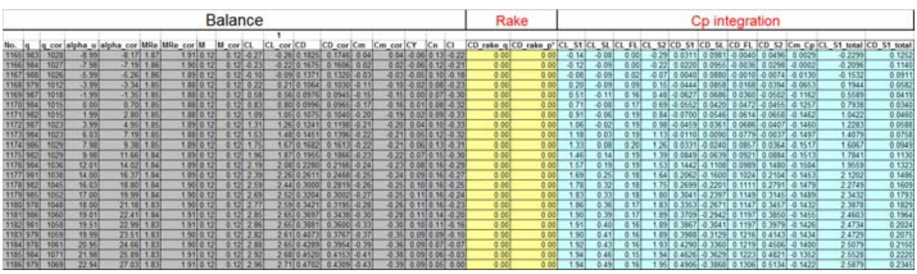

Balance																	
No.	q	q_cor	alpha_u	alpha_cor	MRe	MRe_cor	M	M_cor	CL	CL_cor	CD	CD_cor	Cm	Cm_cor	CY	Cn	Cl
1165	983	1028	-8.99	-8.17	1.87	1.91	0.12	0.12	-0.27	-0.26	0.1825	0.1746	0.04	0.04	-0.06	0.13	-0.22
1166	984	1027	-7.98	-7.19	1.86	1.90	0.12	0.12	-0.23	-0.22	0.1675	0.1606	0.02	0.02	-0.06	0.12	-0.21
1167	988	1026	-5.99	-5.26	1.86	1.89	0.12	0.12	-0.10	-0.09	0.1371	0.1320	-0.03	-0.03	-0.05	0.10	-0.18
1168	979	1012	-3.99	-3.34	1.85	1.88	0.12	0.12	0.22	0.21	0.1064	0.1030	-0.11	-0.10	-0.02	0.08	-0.27
1169	967	1018	-1.99	-1.35	1.85	1.88	0.12	0.12	0.58	0.56	0.0976	0.0945	-0.15	-0.15	0.00	0.07	-0.30
1170	984	1015	0.00	0.70	1.85	1.88	0.12	0.12	0.83	0.80	0.0996	0.0965	-0.17	-0.16	0.01	0.08	-0.32
1171	982	1015	1.99	2.80	1.85	1.88	0.12	0.12	1.09	1.05	0.1075	0.1040	-0.20	-0.19	0.02	0.09	-0.33
1172	987	1023	3.99	4.95	1.85	1.89	0.12	0.12	1.31	1.26	0.1241	0.1198	-0.21	-0.20	0.04	0.10	-0.33
1173	984	1023	6.03	7.19	1.85	1.88	0.12	0.12	1.53	1.48	0.1451	0.1396	-0.22	-0.21	0.05	0.12	-0.32
1174	986	1029	7.98	9.38	1.85	1.89	0.12	0.12	1.75	1.67	0.1682	0.1613	-0.22	-0.21	0.06	0.13	-0.31
1175	982	1029	9.98	11.66	1.84	1.89	0.12	0.12	1.96	1.87	0.1955	0.1866	-0.23	-0.22	0.07	0.15	-0.30
1176	984	1036	12.01	14.02	1.84	1.89	0.12	0.12	2.19	2.08	0.2280	0.2166	-0.24	-0.23	0.08	0.16	-0.29
1177	981	1038	14.00	16.37	1.84	1.89	0.12	0.12	2.39	2.26	0.2611	0.2468	-0.25	-0.24	0.09	0.16	-0.27
1178	982	1045	16.03	18.80	1.84	1.90	0.12	0.12	2.59	2.44	0.3000	0.2819	-0.26	-0.25	0.10	0.16	-0.25
1179	985	1052	17.00	19.99	1.84	1.90	0.12	0.12	2.69	2.52	0.3204	0.3002	-0.27	-0.25	0.11	0.16	-0.24
1180	978	1048	18.00	21.18	1.83	1.90	0.12	0.12	2.77	2.59	0.3421	0.3195	-0.28	-0.26	0.11	0.16	-0.23
1181	986	1060	19.01	22.41	1.84	1.91	0.12	0.12	2.85	2.65	0.3697	0.3438	-0.30	-0.28	0.11	0.14	-0.20
1182	981	1058	19.51	22.99	1.83	1.91	0.12	0.12	2.86	2.65	0.3881	0.3600	-0.33	-0.30	0.10	0.11	-0.16
1183	979	1059	19.99	23.51	1.83	1.90	0.12	0.12	2.82	2.61	0.4073	0.3767	-0.37	-0.35	0.09	0.09	-0.10
1184	978	1061	20.96	24.66	1.83	1.90	0.12	0.12	2.88	2.65	0.4289	0.3954	-0.39	-0.36	0.09	0.07	-0.07
1185	984	1071	21.98	25.89	1.83	1.91	0.12	0.12	2.92	2.68	0.4520	0.4153	-0.41	-0.38	0.09	0.06	-0.03
1186	979	1069	22.94	27.03	1.83	1.91	0.12	0.12	2.96	2.71	0.4702	0.4309	-0.43	-0.39	0.09	0.05	0.00

	Rake		Cp integration										
No.	CD_rake_q	CD_rake_p'	CL_S1	CL_SL	CL_FL	CL_S2	CD_S1	CD_SL	CD_FL	CD_S2	Cm_Cp	CL_S1_total	CD_S1_total
1165	0.00	0.00	-0.14	-0.08	0.00	-0.29	0.0311	0.0981	-0.0040	0.0496	0.0029	-0.2299	0.1252
1166	0.00	0.00	-0.12	-0.09	0.00	-0.22	0.0220	0.0955	-0.0036	0.0298	-0.0002	-0.2096	0.1140
1167	0.00	0.00	-0.08	-0.09	0.02	-0.07	0.0040	0.0880	-0.0010	-0.0074	-0.0130	-0.1532	0.0911
1168	0.00	0.00	0.20	-0.09	0.09	0.15	-0.0444	0.0858	0.0168	-0.0394	-0.0653	0.1944	0.0582
1169	0.00	0.00	0.51	-0.11	0.16	0.48	-0.0627	0.0686	0.0360	-0.0502	-0.1162	0.5589	0.0419
1170	0.00	0.00	0.71	-0.08	0.17	0.69	-0.0552	0.0420	0.0472	-0.0455	-0.1257	0.7938	0.0340
1171	0.00	0.00	0.91	-0.06	0.19	0.84	-0.0700	0.0546	0.0614	-0.0658	-0.1462	1.0422	0.0460
1172	0.00	0.00	1.06	-0.02	0.19	0.98	-0.0459	0.0361	0.0686	-0.0407	-0.1460	1.2283	0.0588
1173	0.00	0.00	1.18	0.03	0.19	1.13	-0.0110	0.0090	0.0779	-0.0037	-0.1497	1.4079	0.0758
1174	0.00	0.00	1.33	0.08	0.20	1.26	0.0331	-0.0240	0.0857	0.0364	-0.1517	1.6067	0.0945
1175	0.00	0.00	1.46	0.14	0.19	1.39	0.0849	-0.0639	0.0921	0.0884	-0.1513	1.7841	0.1130
1176	0.00	0.00	1.57	0.19	0.19	1.53	0.1442	-0.1108	0.0989	0.1480	-0.1504	1.9559	0.1323
1177	0.00	0.00	1.69	0.25	0.18	1.64	0.2062	-0.1600	0.1024	0.2104	-0.1453	2.1202	0.1486
1178	0.00	0.00	1.78	0.32	0.18	1.75	0.2699	-0.2201	0.1111	0.2791	-0.1479	2.2749	0.1609
1179	0.00	0.00	1.83	0.33	0.18	1.80	0.3041	-0.2397	0.1149	0.3145	-0.1489	2.3432	0.1793
1180	0.00	0.00	1.86	0.36	0.17	1.83	0.3353	-0.2671	0.1147	0.3457	-0.1432	2.3878	0.1829
1181	0.00	0.00	1.90	0.39	0.17	1.89	0.3709	-0.2942	0.1197	0.3850	-0.1455	2.4603	0.1964
1182	0.00	0.00	1.91	0.40	0.16	1.89	0.3867	-0.3041	0.1197	0.3979	-0.1426	2.4734	0.2024
1183	0.00	0.00	1.90	0.41	0.16	1.89	0.3988	-0.3129	0.1216	0.4143	-0.1434	2.4729	0.2075
1184	0.00	0.00	1.92	0.43	0.16	1.93	0.4290	-0.3360	0.1219	0.4506	-0.1400	2.5079	0.2150
1185	0.00	0.00	1.94	0.46	0.15	1.94	0.4626	-0.3629	0.1223	0.4821	-0.1352	2.5528	0.2220
1186	0.00	0.00	1.94	0.49	0.16	1.95	0.4906	-0.3868	0.1306	0.5134	-0.1422	2.5879	0.2345

Fig. 7 Typical output of the post-processing routine, for a full polar; also included is the Cp matrix

A better solid wall correction for lift and incidence will use an oblique horse-shoe vortex and its images, to properly represent the wing. A CFD approach is currently running in order to give better solid wall corrections, under the paradigm (2). This can be easiest applied in the case of 2D wings.

$$\begin{Bmatrix} Force \\ Moment \\ Cp \end{Bmatrix}_{cor} = \begin{Bmatrix} Force \\ Moment \\ Cp \end{Bmatrix}_{WT} + \left[\begin{Bmatrix} Force \\ Moment \\ Cp \end{Bmatrix}_{CFD\_\infty} - \begin{Bmatrix} Force \\ Moment \\ Cp \end{Bmatrix}_{CFD\_WT} \right] \tag{2}$$

Pressure distributions

Each pressure port has 100 readings, in time, at a given rate. A 3Σ subroutine is implemented, to filter out the noise due to the electric interference or other sources. The other method to filter the signal is using a subroutine from Labview. However, there is an important difference between results. A third method is manual, using Excel and has been used only to validate the numerical routines. Four mechanical scanivalves are used to read two sections of the main element of the wing and one section for the flap. The principal section is streamlined, while the secondary one is normal to the leading edge. The four mechanical scanivalves are synchronized by a dedicated circuit and use a LabView generated command signal. Balancing and scanning time take about 3 minute, giving a temperature increment of about 0.3K for each angle of attack.

Pressure coefficient is integrated to give CL, CD (pressure contribution) and Cm values. Results are saved in text files ready to be used as input in a spreadsheet. A direct comparison of the balance lift and pitching moment with the pressure derived values can be done. Numerical integration is performed on a specified set of components. A connectivity/coordinates file drives this process.

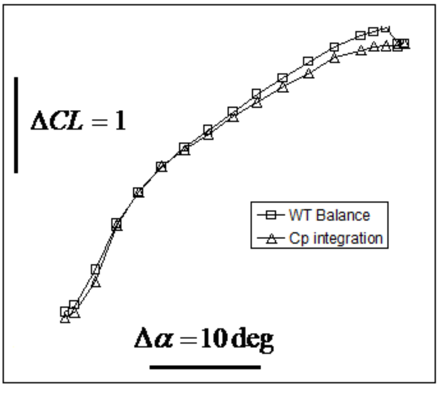

Fig. 8 CL comparison – integrated Cp versus balance corrected measurement

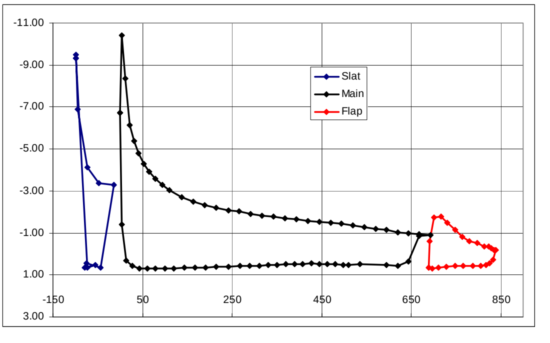

Fig. 9 Setting 19, ME 75% + double slotted flap

Wake rake drag evaluation

Four DSA modules which incorporate 16 temperature compensated piezo-resistive pressure sensors and a microprocessor in a compact self contained module. The microprocessor compensates for temperature changes and performs engineering unit conversion. They are connected in the local area network and have IP assigned. Data stream is read in a LabView routine and then written in a formatted text file. Reading of the 64 channels is simultaneously. Time series of 200 readings are provided and used in the post-processing routine. The 3σ subroutine is again used to filter, this time the aerodynamic noise only. Scanning sequence takes 0.2s. The total pressure captured, was not directly used. Averaged static pressure was subtracted. Integration of the pressure profile doesn't provide good results. A new rake is prepared, containing 6 Pitot-Prandtl probes out of 53 total probes. Local static pressure in the wake seem to have a significant influence in the drag coefficient. Also local flow direction has a strong influence on results.

Preliminary results were negative, due to the important separation of some configurations, important deflection angle as in [4] and the lack of static pressure probes. Wake rake has not been used during the main campaign, because there was no requirement for this type of measurement. A new device is prepared, having 6 Pitot-Prandtl probes and a uniform probe distribution, to keep the same resolution during the incidence sweep, which correspond to a significant movement of the Gaussian velocity profile, see Fig. 10.

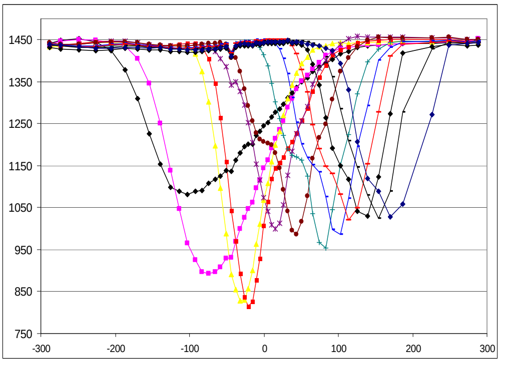

Fig. 10 Dynamic pressure [Pa] vs z coordinate [mm] corresponding to a full incidence sweep, taken with a 53 total heads wake rake

Fig. 11 Total heads rake with Gaussian distribution of probes, in the preliminary phase of WT campaign; large endplates

4. EXPERIMENTAL RESULTS AND CONCLUSIONS

The configuration is quite unusual: swept wing mounted on a three strut balance, having a swept rotation axis. The endplates are streamlined only at 0 deg balance angle. At different incidences they add a significant, yet unknown amount of drag to the balance measurement. The large endplates, designed for the same model in a 2D configuration, provided a very small range of incidence. A strong vibration was remarked at 7 deg balance angle. Smaller elliptic endplates have replaced the first ones. The permissible range of incidence was enlarged, although not enough to reach the stall angle. A third set of narrow endplates, resembling the mean curve of the airfoil, with circular leading and trailing edges were designed and manufactured. They provided a clear improvement and a smoother run of the tests. Still another major improvement has been done, adopting an asymmetric endplate configuration, with the elliptic endplate in the left end, inspired by an isolated trapezoidal wing mounted on a similar 3 strut support, depicted in [8]. The improvements in reducing the induced/parasitic drag of the model, can be clearly seen in Fig. 13. Inverting the asymmetric setup, limited again the alpha range, by serious vibrations.

Vibrations and balance loading limitations prevented the planned velocity of 50m/s, corresponding to Re=2.5M. A velocity of 40m/s, corresponding to Re=2M has been chosen and a Re effect assessment can be seen in Fig. 14. The smaller velocity does not have significant effects.

Fig. 12 SFWA 114 F15 model with large, intermediate and asymmetric (intermediate+small) end plates

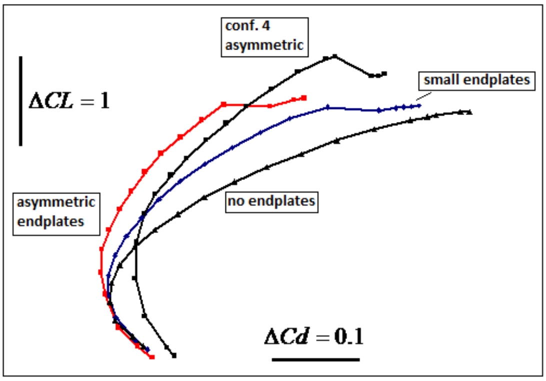

Fig. 13 Endplate effect in induced drag, for reference configuration (take off) and 4th configuration (landing)

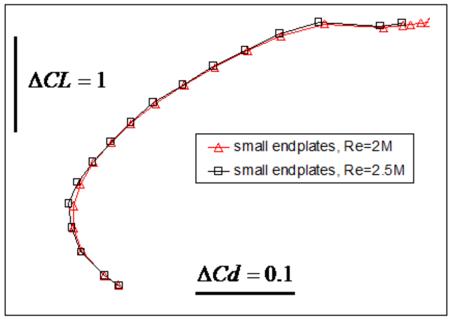

Fig. 14 Re effect on the wing with two small endplates

Polars and pressure distributions

Polars of all 54 configurations are included, as well as tables with uncorrected and corrected data. Solid wall corrected results are presented in Fig. 15.

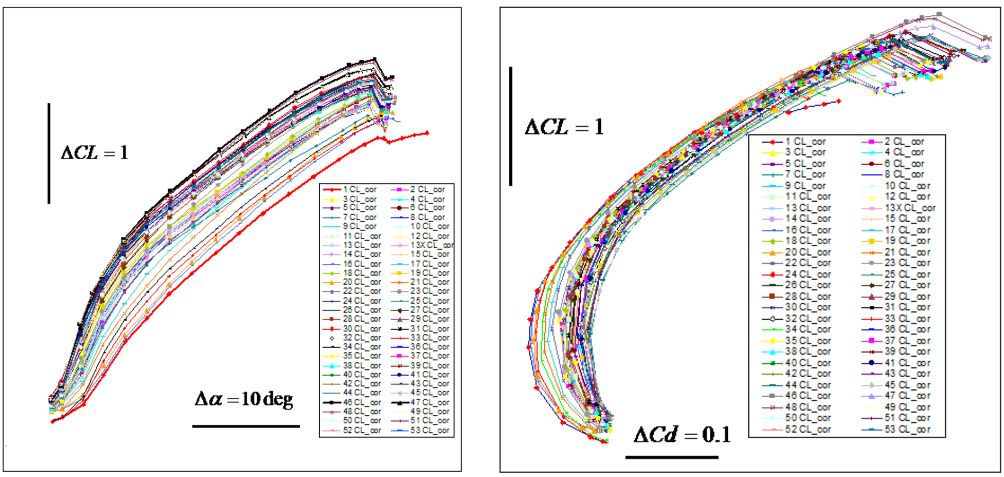

Fig. 15 Lift curves and drag polars for all configurations

The relative difference among all balance measured quantities is in a good agreement with the pressure integration values, proving the overall coherence in this experimental setup/post processing. Unsatisfactorily agreement is in pitching moment, which must be carefully checked.

Trapezoid integration proved to be not enough accurate. More information about curve length and normal vector should be included, in order to improve the accuracy. This is an ongoing effort.

Considerably large lift increments were found using the presented passive configurations, enabling a promising usage for swept wing applications.

- MVG1 (3mm in height) on the flap brought some small gain in CL, around 0.1, only in separated flap configurations. Sublayer MVG3 (1.5 mm in height) brought little improvement. A smaller spacing is to be tested in the future.

- MVGs on the upper panel (MVG2 and MVG4) did not show the expected effect.

- The test results confirmed the interesting characteristic of the max. extension ME concept, where the linear increase of CL with the extension was confirmed both at CL_{max} and in the linear region (0.33 CL increment for 100% max extension).

- The combination of ME 75% and double slotted concept was as efficient in the linear part, but less efficient close to CL_{max}.

- The surprising result was the tab effect which gave 2/3 of the 100% ME effect with far less complexity.

- An even bigger increment of the effect, 0.45 was obtained when combining tab and ME effects, but its feasibility should be checked.

	Reference (Config3) + MVG1	ME 75% (12% extension)	ME 100% (37% extension)	ME 75% + Double Slotted (30° / 20°)	Tab 25% 10° deflected	Tab 25% 30° deflected + MVG1	ME 75% + Tab 25% 20° deflected	ME 100% + Tab 25% 10° deflected
kinematics Complexity	1 DoF	2 DoF	2 DoF	2 DoF	2 DoF	2 DoF	3 DoF	3 DoF
α=12° linear part	0.10	0.08	0.34	0.35	0.25	0.33	0.37	0.46
C_L max	0.07	0.08	0.32	0.27	0.23	0.24	0.31	0.44

Fig. 16 CL increments for families of configurations

Flow visualizations were performed at 10deg AoA and near CL_{max}. Topology of the flow was identified for the main element. A strong vortex appears near the right endplate near CL_{max}.

The same vortex is much smaller at 10 deg. Wakes of slat struts are easily distinguished. Flow orientation is quite evident and it is not perfectly aligned with the main pressure taps row, which also interferes with a slat strut wake. This might have an effect on the efficiency of the main element vortex generators.

Oil-paint visualization in Fig. 17 and Fig. 18 reveals MVG1 effect (3mm in height) on the flap set at 48 deg, corresponding to configuration 43, see Fig. 1.

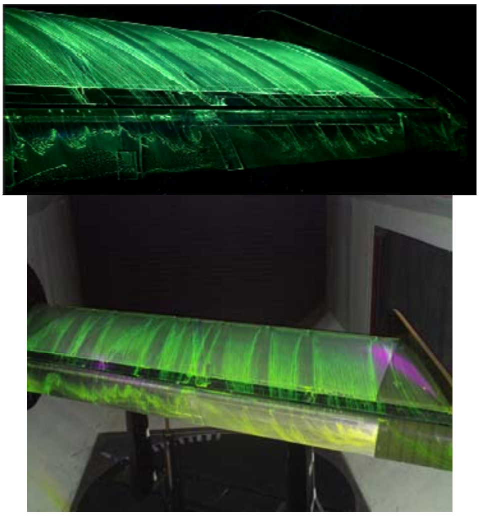

Fig. 17 Flow visualization, Aoa=10 deg

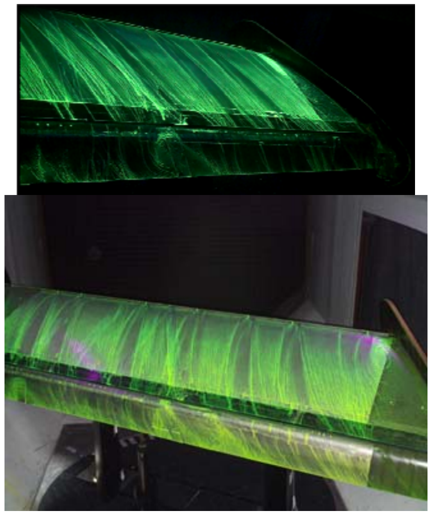

Fig. 18 Flow visualization, Aoa coresponding to CLmax

Output of this activity is used by Dassault Aviation in order to assess a new flap technology for business jet. This work is supported by the Joint Technology Initiative – JTI Clean Sky, SFWA Smart Fixed Wing Aircraft, Work Package 114.

REFERENCES

[1] Octavian Trifu, *Procedura pentru aplicarea corecţiilor de pereţi solizi asupra rezultatelor obţinute la incercările de forţe si momente efectuate in sufleria trisonică in regim subsonic subcritic*, cod I-30.41, 2001, INCAS Internal Report.

[2] Catalin Nae, *Procedura pentru aplicarea corectiilor de suflerie asupra rezultatelor experimentale obţinute în regim subsonic ridicat*, Raport IMFDZ, cod:P-1496, Bucureşti, noiembrie 1994.

[3] B.F.R. Ewald (Editor), AGARDograph 336, *Wind Tunnel Wall Correction, Darmstadt University of Technolog*y, Federal Republic of Germany, 1998, ISBN 92-836-1078-8.

[4] Jochen Wild, *Experimental investigation of Mach- and Reynolds-number dependencies of the stall behaviour of 2-element and 3-element high-lift wing sections*, 50th AIAA Aerospace Sciences Meeting Including the New Horizons Forum and Aerospace Exposition, 09-12 January 2012, Nashville, Tennessee, *AIAA 2012-0108*.

[5] AGARD CONFERENCE PROCEEDINGS 515 *High-Lift System Aerodynamics*, ADVISORY GROUP FOR AEROSPACE RESEARCH & DEVELOPMENT I 2 *7* RUE ANCELLE 92200 NEUILLY SUR SEINE FRANCE.

[6] Alan Pope, Kennith L. Goin, *High-Speed Wind Tunnel Testing*, John Wiley & Sons, Inc., 1965, Library of Congress Card Number: 65-21435.

[7] Al. Marinescu, *Metode, aparate si instalatii de masura in aeromecanica*, Editura Academiei Rpublicii Socialiste Romania, 1970.

[8] Alan Pope, John J. Harper, *Low-Speed Wind Tunnel Testing*, John Wiley & Sons, Inc., 1965, Library of Congress Card Number: 66-17619.

[9] Jean Pierre Rosenblum, *Requirements for INCAS 2.5D test of passive concepts*, Presentation in JTI SFWA WP 1.1.4

[10] J. Wild, G. Wichmann, F. Haucke, I. Peltzer and P. Scholz, "Large scale separation flow control experiments within the German Flow Control Network," *AIAA Paper 2009-0530*, 2009.